

# Quadrupole collectivity beyond $N = 28$ : Intermediate-energy Coulomb excitation of <sup>47,48</sup>Ar

R. Winkler,<sup>1,\*</sup> A. Gade,<sup>1,2</sup> T. Baugher,<sup>1,2</sup> D. Bazin,<sup>1</sup> B. A. Brown,<sup>1,2</sup> T. Glasmacher,<sup>1,2</sup> G. F. Grinyer,<sup>1,†</sup> R. Meharchand,<sup>1,2,\*</sup> S. McDaniel,<sup>1,2</sup> A. Ratkiewicz,<sup>1,2</sup> and D. Weisshaar<sup>1</sup>

<sup>1</sup>*National Superconducting Cyclotron Laboratory, Michigan State University, East Lansing, Michigan 48824, USA*

<sup>2</sup>*Department of Physics and Astronomy, Michigan State University, East Lansing, Michigan 48824, USA*

(Dated: September 22, 2018)

We report on the first experimental study of quadrupole collectivity in the very neutron-rich nuclei <sup>47,48</sup>Ar using intermediate-energy Coulomb excitation. These nuclei are located along the path from doubly-magic Ca to collective S and Si isotopes, a critical region of shell evolution and structural change. The deduced  $B(E2)$  transition strengths are confronted with large-scale shell-model calculations in the *sdpf* shell using the state-of-the-art SDPF-U and EPQQM effective interactions. The comparison between experiment and theory indicates that a shell-model description of Ar isotopes around  $N = 28$  remains a challenge.

Developing predictive power for the fundamental properties of atomic nuclei is driving experimental and theoretical research worldwide. Single-particle motion in a defined nuclear potential is one of the crucial building blocks for a comprehensive picture of these strongly interacting fermionic quantum many-body systems. Large stabilizing energy gaps occur between groups of single-particle states at certain, “magic” fillings with protons or neutrons. The nuclear potential and resulting shell structure have been established in the valley of stability, however, dramatic modifications to the familiar ordering of single-particle orbits in “exotic” nuclei with a large imbalance of proton and neutron numbers have been found: new shell gaps develop and conventional magic numbers break down. Current efforts in nuclear physics are aimed at unraveling the driving forces behind those structural modifications, which are most pronounced in neutron-rich species [1–3].

The neutron magic number  $N = 28$  has attracted much attention in recent years. On the neutron-rich side of the nuclear chart, below doubly magic <sup>48</sup>Ca<sub>28</sub>, the  $N = 28$  shell closure was shown to disappear progressively below  $Z = 20$  in <sup>44</sup>S<sub>28</sub> [4] and <sup>42</sup>Si<sub>28</sub> [5], however, with conflicting experimental data on <sup>46</sup>Ar<sub>28</sub> [6–8]. Much of the initial spectroscopic information referenced above stems from measurements of the energy of the first  $2^+$  state,  $E(2^+_1)$ , and the absolute  $B(E2; 0^+_1 \rightarrow 2^+_1) \equiv B(E2 \uparrow)$  quadrupole excitation transition strength. These observables can signal the breakdown or persistence of a magic number, with high  $E(2^+_1)$  and low  $B(E2 \uparrow)$  values at a shell gap (reduced collectivity) and the reverse in the middle of a shell (collective character or deformation).

The role of the Ar isotopes around  $N = 28$  is of great interest. They are, with  $Z = 18$ , between doubly-magic <sup>48</sup>Ca and the already collective S isotopes ( $Z = 16$ ) on the path to <sup>42</sup>Si, which has the lowest-energy  $2^+_1$  state along the  $N = 28$  isotonic chain to date. Early intermediate-energy Coulomb excitation measurements [4, 6] showed that <sup>40,42,44</sup>S are collective with

high  $B(E2 \uparrow)$  values while, in two independent measurements, the  $B(E2 \uparrow)$  value for <sup>46</sup>Ar was found low as one would expect for a persisting  $N = 28$  shell gap [6, 7]. Shell-model calculations were unable to explain the reduced collectivity in <sup>46</sup>Ar [9, 10] and rather predict the breakdown of  $N = 28$  as a magic number and an onset of collectivity already in Ar. A recent, marginal-statistics excited-state lifetime measurement extracted a much higher  $B(E2 \uparrow)$  value in agreement with the shell-model description [8].

Here, we present the first study of quadrupole collectivity in the  $N = 30, 29$  Ar isotopes <sup>48,47</sup>Ar with intermediate-energy Coulomb excitation. Measured  $B(E2; 0^+_1 \rightarrow 2^+_1)$  and  $B(E2; 3/2^- \rightarrow J)$  values are compared to state-of-the-art shell model calculations, taking into account possible effects of large neutron excess.

Little is known about the  $N = 30$  isotones in even- $Z$  nuclei below <sup>50</sup>Ca. In 2007, <sup>44</sup>Si was proven to be bound [11], and in 2009 excited states in <sup>46</sup>S were first observed using in-beam  $\gamma$ -ray spectroscopy following nucleon-exchange reactions [12]. Excited states in <sup>48</sup>Ar were studied in 2008 with deep-inelastic reactions [13] and in 2009 with nucleon-exchange reactions [12]. Rare-isotope beams in this region of the nuclear chart are typically produced by the fragmentation of a primary <sup>48</sup>Ca beam on a light target. In this scheme, the production of exotic projectiles with  $N = 30, 29$  necessarily involves neutron pickup and/or nucleon exchange processes which proceed with small cross sections compared to reactions that only involve proton or neutron removals. Here we show that, in spite of the small production cross sections, <sup>47,48</sup>Ar projectile beams can be produced from a <sup>48</sup>Ca primary beam at intensities sufficient for  $\gamma$ -ray tagged, thick target intermediate-energy Coulomb excitation measurements, allowing for the study of quadrupole collectivity in these very neutron-rich systems.

The measurements were performed at the Coupled Cyclotron Facility at NSCL on the campus of Michigan State University. The secondary projectile beam con-

taining  $^{47,48}\text{Ar}$  was produced from a 140 MeV/u  $^{48}\text{Ca}$  stable primary beam impinging on a 681 mg/cm<sup>2</sup>  $^9\text{Be}$  production target and separated using a 195 mg/cm<sup>2</sup> Al wedge degrader in the A1900 fragment separator [14]. The total momentum acceptance of the separator was restricted to 2%. The resulting rare-isotope beam was composed of 6.5%  $^{48}\text{Ar}$  and 57%  $^{47}\text{Ar}$ . Typical rates of 150  $^{48}\text{Ar}$ /second and 1300  $^{47}\text{Ar}$ /second were delivered to the experimental end station.

At the pivot point of NSCL's S800 spectrograph [15], a gold target of 518 mg/cm<sup>2</sup> thickness was surrounded by the Segmented Germanium Array (SeGA) consisting of 32-fold segmented high-purity germanium detectors for high-resolution  $\gamma$ -ray spectroscopy [16]. The segmentation allows for event-by-event Doppler reconstruction of  $\gamma$  rays emitted in flight by the scattered projectiles. For this, the  $\gamma$ -ray emission angle entering the Doppler reconstruction is determined from the location of the detector segment with the largest energy deposited. Sixteen detectors were arranged in two rings with central angles of 90° and 37° with respect to the beam axis. The 37° ring was equipped with seven detectors while nine detectors occupied 90° positions. The photopeak efficiency of the array was measured with a  $^{152}\text{Eu}$  standard calibration source and corrected for target absorption and the Lorentz boost of the  $\gamma$ -ray angular distribution emitted by nuclei moving at velocities of more than  $v/c = 0.4$ .

Scattered projectiles were identified on an event-by-event basis using the focal-plane detection system of the large-acceptance S800 spectrograph [15]. The ion's energy loss measured in the S800 ionization chamber and flight-time information measured with two plastic scintillators – corrected for the angle and momentum of each ion – were used to unambiguously identify the scattered projectiles emerging from the target. The identification spectrum is shown in Fig. 1.

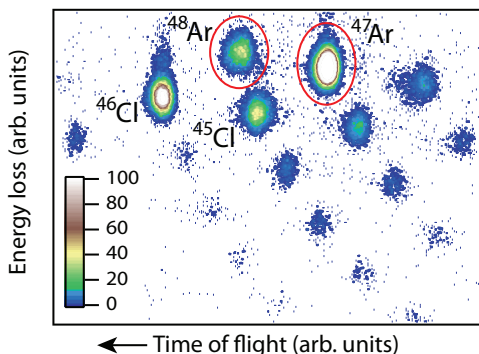


FIG. 1. (Color online) Particle-identification spectrum for the neutron-rich projectile beam passing through the Au target. The energy loss measured in the S800 ionization chamber is plotted versus the ion's flight time.  $^{47}\text{Ar}$  and  $^{48}\text{Ar}$  can be unambiguously identified among the other species in the cocktail beam.

In intermediate-energy Coulomb excitation [3, 17, 18], projectiles are scattered off stable high- $Z$  targets and are detected in coincidence with the de-excitation  $\gamma$  rays, tagging the inelastic process. Very peripheral collisions are selected in the regime of intermediate beam energies to exclude nuclear contributions to the electromagnetic excitation process. This is typically accomplished by restricting the data analysis to events at very forward scattering angles, corresponding to large impact parameters,  $b$ , in the interaction between projectile and target nuclei – here, we chose  $b > 1.2A_p^{1/3} + 1.2A_t^{1/3}$ . Position measurements from the cathode readout drift chambers in the S800 focal plane were combined with ion optics information to reconstruct the projectile's scattering angle on an event-by-event basis. The angle-integrated Coulomb excitation cross section,  $\sigma(\theta_{\text{lab}} \leq \theta_{\text{lab}}^{\text{max}}) \equiv \sigma$ , was determined from the efficiency-corrected  $\gamma$ -ray intensity relative to the number of projectiles per number density of the target and translated into absolute  $B(\sigma\lambda)$  excitation strengths using the Winther-Alder theory of intermediate-energy Coulomb excitation [19].

For the present analysis we use maximum scattering angles of  $\theta_{\text{lab}}^{\text{max}} = 1.94(5)^\circ$  and  $1.97(5)^\circ$  for  $^{47}\text{Ar}$  (100/u MeV mid-target energy) and  $^{48}\text{Ar}$  (96/u MeV mid-target energy), respectively, corresponding to minimum impact parameters just above  $b_{\text{min}} = 13.3$  fm for both projectile-target systems. The event-by-event Doppler-reconstructed  $\gamma$ -ray spectra taken in coincidence with  $^{48,47}\text{Ar}$  – with the scattering-angle restrictions applied – are shown in Fig. 2. The  $\gamma$ -ray transition at 1040 keV observed in  $^{48}\text{Ar}$  is attributed to the decay of the first  $2^+$  state, in agreement with [12, 13]. The  $\gamma$ -ray transition apparent at 1227 keV in the spectrum of  $^{47}\text{Ar}$  is assigned to the decay of the first excited  $5/2^-$  state to the  $3/2^-$  ground state, following [13, 20]. The peak-like structure at about 820 keV in the  $^{48}\text{Ar}$  spectrum is an artefact from Doppler-reconstructed background lines, only seen in the 37° ring of SeGA. Similar structures at the same energy are visible in the spectrum of  $^{47}\text{Ar}$ .

An angle-integrated Coulomb excitation cross section of  $\sigma(^{48}\text{Ar}) = 74(11)$  mb was derived for the excitation of the first  $2^+$  state of  $^{48}\text{Ar}$ , translating into  $B(E2; 0_1^+ \rightarrow 2_1^+) = 346(55) e^2\text{fm}^4$  for this most neutron-rich Ar isotope studied with this technique. The cross section includes statistical uncertainties and a 5% uncertainty on the in-beam  $\gamma$ -ray detection efficiency. For the extracted  $B(E2)$  values, an additional 5% systematic uncertainty originating from the the projectile's scattering angle reconstruction was added in quadrature.

The Coulomb excitation of the odd- $N$   $^{47}\text{Ar}$  is more complicated. A mixed  $E2/M1$  multipolarity is expected for the  $5/2^- \rightarrow 3/2^-$   $\gamma$ -ray transition. The multipole character of the radiation affects the  $\gamma$ -ray angular distribution and thus the detection efficiency. Large-scale shell model calculations with different interactions, SDPF-U [10] and EPQQM [21], compute an identical multipole

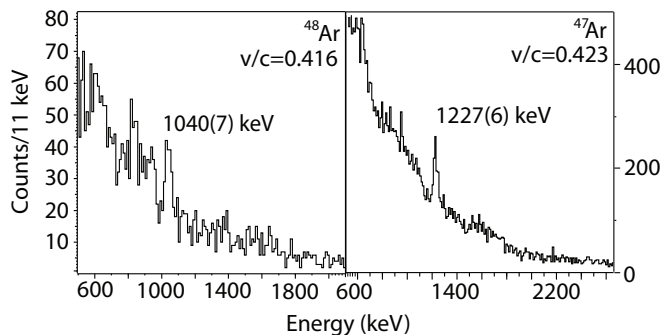


FIG. 2. Event-by-even Doppler reconstructed  $\gamma$ -ray spectra detected in coincidence with scattered  $^{48}\text{Ar}$  (left) and scattered  $^{47}\text{Ar}$  (right). Gamma-ray transitions at 1040 keV and 1227 keV can be clearly identified and are attributed to the de-excitation  $\gamma$  rays from the first excited  $2^+$  state in  $^{48}\text{Ar}$  and the first excited  $5/2^-$  state in  $^{47}\text{Ar}$ , respectively.

mixing ratio of  $\delta(E2/M1) = 1.01$ , corresponding to 50%  $M1$  character. This  $\delta(E2/M1)$  was used in the determination of the in-beam detection efficiency of SeGA. To put this into perspective, assuming 100%  $E2$  character would only introduce a relative change of 1.5% in the detection efficiency. However, in the excitation process,  $E2$  multipolarity dominates over  $M1$  by orders of magnitude, with 20.9 mb/100  $e^2\text{fm}^4$  and 0.18 mb/0.1  $\mu_N^2$  for Coulomb excitation via  $E2$  and  $M1$ , respectively. Shell-model calculations predict  $B(M1; 3/2^- \rightarrow 5/2^-) = 0.0236 \mu_N^2$  (SDPF-U) [10] or less (EPQQM) [21] and we thus assume that the excitation proceeds solely via  $E2$  character.  $B(E2; 3/2^- \rightarrow 5/2^-) = 135(17) e^2\text{fm}^4$  is deduced from the measured cross section of  $\sigma(^{47}\text{Ar}) = 28(3)$  mb, with an error budget as detailed for  $^{48}\text{Ar}$ .

The consistent description of the onset of collectivity at  $N = 28$  in the isotopic chains of sulfur ( $Z = 16$ ) and silicon ( $Z = 14$ ) has been a challenge for large-scale shell-model calculations and was accomplished by Nowacki and Poves by devising two effective interactions (SDPF-U) for the *sd*pf model space, one valid for  $Z \leq 14$  and one to be applied for  $Z > 14$  [10]. In a recent shell-model work by Kaneko *et al.*, the extended pairing plus quadrupole-quadrupole force with inclusion of a monopole interaction (EPQQM) was proposed to provide a consistent description of the breakdown of  $N = 28$  across the  $Z = 20$  to  $Z = 14$  isotopic chains [21]. Both shell-model interactions use  $e_p = 1.5e$  and  $e_n = 0.5e$  for the effective charges that enter the computation of  $B(E2)$  transition strengths from the proton and neutron shell-model transition amplitudes  $A_p$  and  $A_n$  via  $B(E2; J_i \rightarrow J_f) = (e_n A_n + e_p A_p)^2 / (2J_i + 1)$ . In Fig. 3 (upper panel), the shell model  $B(E2; 0_1^+ \rightarrow 2_1^+)$  values calculated with the two different effective interactions – using the standard effective charges quoted above – are compared to the available measured values in the chain of Ar isotopes, starting from semi-magic  $^{38}\text{Ar}_{20}$  [6–8, 23].

The two calculations describe the trend of the data on the even-even isotopes well only if one neglects the two consistent, low  $B(E2 \uparrow)$  values at  $N = 28$  [6, 7] and assumes that the marginal-statistics excited-state lifetime measurement for  $^{46}\text{Ar}$  is correct – with small differences in the detailed trends of the two calculations. For  $^{48}\text{Ar}$  the calculation is within 2 sigma of the experimental value for the SDPF-U effective interaction. The EPQQM effective interaction differs somewhat in the trend approaching  $N = 28$ , with a marked drop in the  $B(E2 \uparrow)$  strength at  $N = 26$  that is not present in the SDPF-U results but consistent with the data. For  $^{48}\text{Ar}$ , the EPQQM calculation is within 1.5 sigma of the measured value. The trend beyond  $N = 30$  is predicted very differently by the two interactions, with rather constant  $B(E2 \uparrow)$  values out to  $N = 34$  for the SDPF-U interaction and a rise in collectivity for EPQQM, with  $^{52}\text{Ar}_{34}$  being the most collective in the chain. The calculated  $E(2_1^+)$  energies reproduce the measured energies well where available, with the SDPF-U and EPQQM predictions diverging at  $N = 34$ . At  $N = 28$ , both calculations predict high  $B(E2 \uparrow)$  and  $E(2_1^+)$  values, deviating from established systematics [22] that rather suggests their anti-correlation as observed for  $^{38}\text{Ar}_{20}$ , for example.

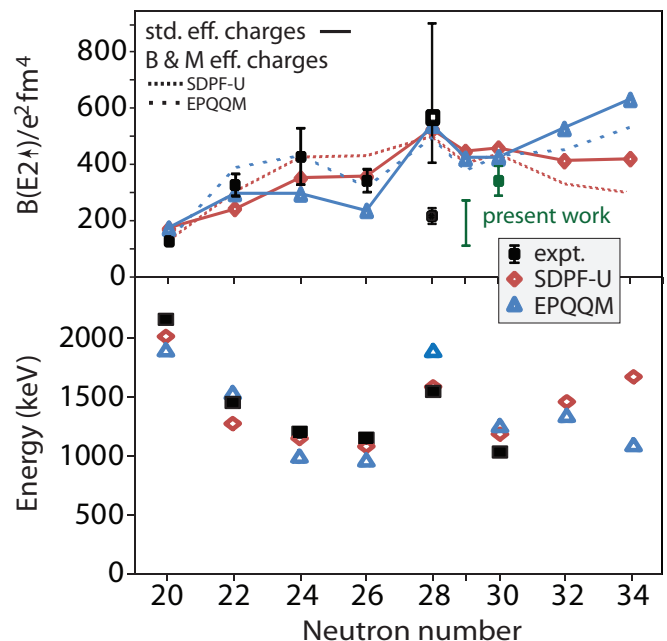


FIG. 3. (Color online) (upper panel) Measured  $B(E2 \uparrow)$  for the chain of Ar isotopes [6–8, 23] compared to shell-model calculations using two different effective interactions with the standard effective charges,  $e_p = 1.5e$  and  $e_n = 0.5e$  (solid lines) and  $N, Z$ -dependent effective charges following Bohr and Mottelson (dashed lines). (lower panel) Measured and calculated  $E(2_1^+)$  energies for the Ar isotopic chain.

The question arises as to the effects of neutron excess on the transition strength. The effective charges, which generally compensate for missing excitations beyond the

(necessarily) limited model space, can be formulated following Bohr and Mottelson [24] to explicitly include neutron excess via  $e_n^{BM} = e_{pol}$  and  $e_p^{BM} = 1 + e_{pol}$  where  $e_{pol} = e(Z/A - 0.32(N-Z)/A + (0.32 - 0.3(N-Z)/A)\tau_z)$  is the polarization charge with  $\tau_z = 1, -1$  for neutrons and protons, respectively. This approach approximates the coupling of the particle motion to higher frequency quadrupole modes that are beyond the model spaces of the effective shell-model interactions [24]. Figure 3 confronts the experimental data with the shell-model  $B(E2 \uparrow)$  values calculated with  $e_{p,n} = 1.14 e_{p,n}^{BM}$  (dashed line). A slight renormalization of the effective charges by 1.14 was introduced to have the results with both interactions reproduce the  $B(E2 \uparrow)$  value of semi-magic  $^{38}\text{Ar}$ . With the calculations anchored in this way and the effective charges evolving with neutron excess, subtle changes in the theory trends are visible. The description of the available data by the EPQQM effective interaction improved, in particular below  $N = 28$ , and the quality of the SDPF-U calculation remains roughly the same. The differing trend beyond  $N = 30$  is amplified, with a larger discrepancy in the prediction of the  $B(E2 \uparrow)$  value at  $N = 34$ . If the low  $B(E2 \uparrow)$  value for  $^{46}\text{Ar}$  should be proven correct, certainly the modified effective charges would not reverse the trend at  $N = 28$  and leave a striking disagreement between experiment and shell model as to the evolution of collectivity below  $^{48}\text{Ca}$  towards  $^{42}\text{Si}$ .

With conflicting experimental results at  $^{46}\text{Ar}$  and rather robust shell-model calculations at  $N = 28$ , it is interesting to turn to the odd- $N$  neighbor  $^{47}\text{Ar}$ . In odd- $A$  nuclei, core-coupled states are expected to carry the  $E2$  strength. These states can be qualitatively described as originating from a particle or hole weakly coupled to the neighboring even-even core [25]. For  $^{47}\text{Ar}$ , the coupling of the odd  $p_{3/2}$  proton to the  $^{46}\text{Ar}$   $2_1^+$  state would give rise to a quartet of states with spin values of  $1/2^-$ ,  $3/2^-$ ,  $5/2^-$ , and  $7/2^-$  at about  $E(2_1^+ (^{46}\text{Ar})) = 1555$  keV [7] and with a total  $E2$  excitation strength of  $\Sigma_J B(E2; 3/2^- \rightarrow J) = B(E2 \uparrow)_{^{46}\text{Ar}}$ . Indeed, in both shell model calculations, the lowest-lying  $1/2^- - 7/2^-$  excited states are found between 1139 - 2125 keV and 950 - 2343 keV in the SDPF-U and EPQQM calculations, respectively. As one would expect in this extreme weak-coupling scheme, 85.0% and 99.7% of the shell-model  $B(E2 \uparrow)_{^{46}\text{Ar}}$  are exhausted by this multiplet in the respective interactions.

In the present measurement, there is only clear evidence for one strongly excited state, at 1227 keV with alleged  $5/2^-$  spin assignment [13, 20]. Using the  $^{47}\text{Ar}$  level scheme presented in [13, 20], and assuming that the observed 1747 keV and 2190 keV states are the  $7/2^-$  and  $3/2^-$  members of the multiplet, we can establish upper limits for the  $B(E2)$  excitation strengths in the present work (we neglect the  $1/2^-$  member of the multiplet as this state is expected to be only weakly excited). From the  $\gamma$ -ray spectrum of [13], we roughly estimated 60% and 40% branches to the ground state

and the alleged  $5/2^-$  first excited state, respectively, for both states. We estimated a possible maximum number of  $\gamma$ -ray counts in the expected transitions to the ground state and – taking into account the assumed branching ratios – extract upper limits of  $\sigma(7/2^-) \leq 16(8)$  mb and  $\sigma(3/2^-) \leq 4(2)$  mb with conservative 50% uncertainties, translating into generous upper limits of  $B(E2; 3/2^- \rightarrow 7/2^-) < 74(37) e^2\text{fm}^4$  and  $B(E2; 3/2^- \rightarrow 3/2^-) < 20(10) e^2\text{fm}^4$  for the  $E2$  excitation strength. In Fig. 4, the measured  $B(E2)$  values and limits are compared to the two shell model calculations (with standard effective charges). First, this comparison supports the assignment of the level at 1227 keV as the  $5/2^-$  state, which – in both calculations – is predicted to carry the largest fraction of the  $E2$  excitation strength. We note that the EPQQM interaction predicts the centroid of the  $E2$  strength to lie about 500 keV higher than in the SDPF-U calculation.

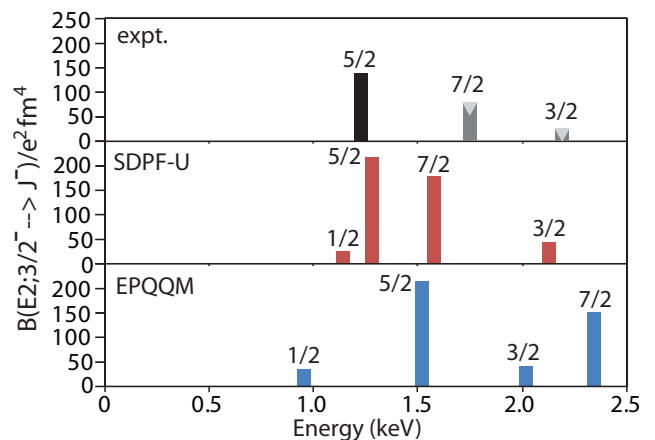


FIG. 4.  $B(E2; 3/2^- \rightarrow J^-)$  strength distribution for the lowest-lying excited  $1/2^- - 7/2^-$  states. The experimental values for  $J = 7/2$  and  $3/2$  are upper limits as described in the text. Standard effective charges were used in both shell-model calculations.

The total  $\Sigma_J B(E2; 3/2^- \rightarrow J^-)$  strength concentrated in these states is included in the  $B(E2)$  systematics of Fig. 3 at  $N = 29$  for experiment as well as theory. The comparison shows that both shell-model effective interactions significantly overpredict the  $B(E2)$  strength concentrated in the low-lying states of  $^{47}\text{Ar}$ . The experimental  $B(E2)$  range given in the figure marks the possible span of the total  $B(E2)$  strength ranging from the sole excitation of the  $5/2^-$  states to the maximum strength observed in case the upper limits for the excitation of the  $7/2^-$  and  $3/2^-$  members of the quartet should be realized. This discrepancy is consistent with the situation at  $N = 28$  if the measured low  $B(E2 \uparrow)$  value for  $^{46}\text{Ar}$  should be proven correct. This result for  $^{47}\text{Ar}$  indicates that challenges remain for the most modern shell-model effective interactions in this area of rapid structural change and it also demonstrates the seldom exploited, sensitive benchmark posed by measures of col-

lectivity in odd- $A$  nuclei.

In summary, we studied the quadrupole collectivity in the very neutron-rich nuclei  $^{47,48}\text{Ar}$  via intermediate-energy Coulomb excitation. While the two most recent effective shell-model effective interactions predict  $B(E2 \uparrow)$  values for  $^{48}\text{Ar}$  close to the experimental result, the low-lying quadrupole collectivity in  $^{47}\text{Ar}$  is significantly overpredicted by theory, reminiscent of the situation in  $^{46}\text{Ar}$  if the lower of the conflicting  $B(E2 \uparrow)$  values in the literature should be proven correct. We show that modified effective charges that approximate effects of neutron excess do not resolve the discrepancy at  $N = 28, 29$  in the Ar isotopes and demonstrate the potential of studies of quadrupole collectivity in odd- $A$  nuclei to sensitively probe nuclear structure calculations.

This work was supported by the National Science Foundation under Grants No. PHY-0606007, PHY-1102511 and PHY-1068217. A. G. is supported by the Alfred P. Sloan Foundation.

---

\* Present address: Los Alamos National Laboratory, Los Alamos, NM 87545, USA

† Present Address: Grand Accélérateur National d'Ions Lourds (GANIL), CEA/DSM-CNRS/IN2P3, Bvd Henri Becquerel, 14076 Caen, France

[1] B.A. Brown, Prog. Part. Nucl. Phys. 47, 517 (2001).

[2] O. Sorlin and M.-G. Porquet, Prog. Part. Nucl. Phys. 61,

602 (2008).

[3] A. Gade and T. Glasmacher, Prog. Part. Nucl. Phys. 60, 161 (2008).

[4] T. Glasmacher *et al.*, Phys. Lett. 395, 163 (1997).

[5] B. Bastin *et al.*, Phys. Rev. Lett. 99, 022503 (2007).

[6] H. Scheit *et al.*, Phys. Rev. Lett. 77, 3967 (1996).

[7] A. Gade *et al.*, Phys. Rev. C 68, 014302 (2003).

[8] D. Mengoni *et al.*, Phys. Rev. C 82, 024308 (2010).

[9] S. Nummela *et al.*, Phys. Rev. C 63, 044316 (2001).

[10] F. Nowacki and A. Poves, Phys. Rev. C 79, 014310 (2009).

[11] O. B. Tarasov *et al.*, Phys. Rev. C 75, 064613 (2007).

[12] A. Gade *et al.*, Phys. Rev. Lett. 102, 182502 (2009).

[13] S. Bhattacharyya *et al.*, Phys. Rev. Lett. 101, 032501 (2008).

[14] D. J. Morrissey *et al.*, Nucl. Instrum. Methods in Phys. Res. B 204, 90 (2003).

[15] D. Bazin *et al.*, Nucl. Instrum. Methods in Phys. Res. B 204, 629 (2003).

[16] W. F. Mueller *et al.*, Nucl. Instrum. and Methods in Phys. Res. A 466, 492 (2001).

[17] T. Motobayashi *et al.*, Phys. Lett. B346, 9 (1995).

[18] T. Glasmacher, Annu. Rev. Nucl. Part. Sci. 48, 1 (1998).

[19] A. Winther and K. Alder, Nucl. Phys. A319, 518 (1979).

[20] L. Gaudefroy *et al.*, Phys. Rev. Lett. 97, 092501 (2006).

[21] K. Kaneko, Y. Sun, T. Mizusaki, and M. Hasegawa, Phys. Rev. C 83, 014320 (2011).

[22] S. Raman, C. W. Nestor, and P. Tikkanen, At. Data Nucl. Data Tables 78, 1 (2001).

[23] S. Raman, C. W. Nestor, and P. Tikkanen, At. Nucl. Data Tables 78, 1 (2001).

[24] A. Bohr and B.R. Mottelson, Nuclear Structure (W. A. Benjamin, Massachusetts, 1975), Vol. 2, p. 515.

[25] A. Arima and I. Hamamoto, Annu. Rev. Nuc. Sci. 21, 55 (1971).